

Observation of Negative Magnetoresistance and nontrivial π Berrys phase in 3D Weyl semi-metal NbAs

Xiaojun Yang,¹ Yupeng Li,¹ Zhen Wang,¹ Yi Zhen,^{1,2,*} and Zhu-an Xu^{1,2,†}

¹*Department of Physics and State Key Laboratory of Silicon Materials, Zhejiang University, Hangzhou 310027, China*

²*Collaborative Innovation Centre of Advanced Microstructures, Nanjing 210093, P. R. China*

(Dated: June 9, 2015)

We report the electric transport properties of NbAs, which is a Weyl semimetal candidate proposed by recent theoretical calculations and confirmed by recent angle-resolved photoemission spectroscopy (ARPES) data. We detected the long-anticipated negative magneto-resistance generated by the chiral anomaly in NbAs. Clear Shubnikov de Haas (SdH) oscillations have been detected starting from very weak magnetic field. Analysis of the SdH peaks gives the Berry phase accumulated along the cyclotron orbits to be π , indicating the existence of Weyl points.

PACS numbers: 71.55.Ak, 71.70.Di, 72.15.Gd

Predicted to show unprecedented features beyond the classical electronic theories of metals, Weyl semi-metal (WSM) has motivated much interest for the realization of electronic topological properties. The appearance of Weyl points near the Fermi level will cause novel properties¹⁻⁶. For materials with Weyl points located near the Fermi level, called as Weyl semi-metals, exotic low energy physics will be expected, such as the Fermi arcs on the surfaces^{7,8}, and the chiral-anomaly induced quantum transport^{1,9,10}. The band crossing points in WSMs, i.e. Weyl nodes, always appear in pair with opposite chirality, due to the lifting of spin degeneracy by breaking symmetry^{7,11}. By symmetry breaking, a 3D Dirac semimetal can be driven to a Weyl semimetal or topological insulator¹². As a 3D analogue to graphene, the 3D Weyl semimetal could be important for future device applications.

The chiral anomaly in WSM will in general lead to negative magneto-resistance ($MR = [\rho(H) - \rho(0)]/\rho(0)$) when the magnetic field is parallel to the current^{10,13}. For ordinary metal or semiconductors the MR is weak, positive and usually not very sensitive to the magnetic field direction. The negative and highly anisotropic MR has been regarded as the most prominent signatures in transport for the chiral anomaly and indicates the existence of 3D Weyl points¹⁰. Another distinguished feature of Dirac fermions and Weyl fermions is the nontrivial π Berrys phase, which results from their cyclotron motion^{14,15}. It is a geometrical phase factor, acquired when an electron circles a Dirac point. This Berrys phase can be experimentally accessed by analyzing the Shubnikovde Haas (SdH) oscillations, which has been widely employed in 2D graphene^{16,17}, bulk Rashba Semiconductor BiTeI¹⁸, bulk SrMnBi₂ in which highly anisotropic Dirac fermions reside in the 2D Bi square net¹⁹, 3D Dirac Fermions Cd₃As₂²⁰, and recently in Weyl semi-metal TaAs^{10,21}.

Recently, using first principle calculations, Weng et al. predicted that non-centrosymmetric TaAs, TaP, NbAs and NbP, are time-reversal invariant 3D WSMs with a dozen pairs of Weyl nodes which are generated by the absence of inversion center¹¹. The proposal have stim-

ulated enormous interests. The existence of Weyl nodes has soon been discovered in TaAs by angle-resolved photoemission spectroscopy (ARPES)^{22,23}, and by quantum transport measurements of negative MR and a non-trivial π Berrys phase^{10,21}. Transport studies of NbAs also show ultrahigh mobility and non-saturating MR²⁴, but no negative MR and a non-trivial π Berrys phase are acquired. However, very recent ARPES results detecte Weyl cones and Weyl nodes in the bulk and the Fermi arcs on the surface of NbAs²⁵. Observation of Negative Magnetoresistance and nontrivial π Berrys phase in 3D Weyl semi-metal NbAs.

Niobium arsenide, NbAs, crystallizes in a body-centered tetragonal Bravais lattice, space group I4₁md (109). Our X-ray diffraction (XRD) obtains lattice constants of $a = 3.45 \text{ \AA}$ and $c = 11.68 \text{ \AA}$, consistent with the earlier crystallographic studies²⁵⁻²⁷. Single crystals of NbAs were grown by vapor transport using iodine as the transport agent, as described in Ref.²⁴. First, polycrystalline NbAs was prepared by heating stoichiometric amounts of Nb and As in an evacuated silica ampoule at 973 K for 1 day. Subsequently, the powder was loaded in a horizontal tube furnace in which the temperature of the hot zone was kept at 1223 K and that of the cold zone was at 1123 K. The crystals of NbAs were verified by powder x-ray diffraction (XRD) and by compositional analysis conducted using an energy dispersive x-ray spectroscopy (EDS). An atomic percentage ratio of Nb:As = 49.4 : 50.6 was obtained on the EDS measurements. The largest natural surface of the obtained NbAs single crystals was determined to be the (112) plane by single crystal x-ray diffraction, shown in the lower inset of Fig. 1(a), with typical dimension of $1 \times 1 \text{ mm}^2$. The quality of the NbAs single crystals was further checked by the x-ray rocking curve. The full width at half maximum (FWHM) is only 0.03° (not showing here), indicating the high quality of the single crystals. The sample was polished to a bar shape, with $1 \times 0.3 \text{ mm}^2$ in the (112) plane and a 0.2 mm thickness. A standard six-probe method was used for both the longitudinal resistivity and transverse Hall resistance measurements.

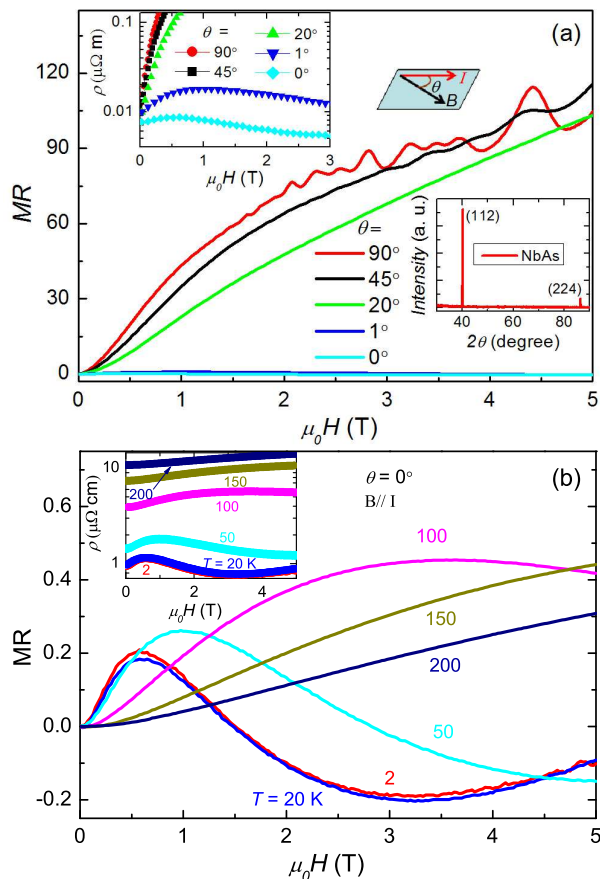


FIG. 1: (Color online) (a), Magnetic field dependence of Magnetoresistance with magnetic field (μ_0H) from perpendicular ($\theta = 90^\circ$) to parallel ($\theta = 0^\circ$) to the electric current (I) at $T = 2$ K. The upper left inset displays the original resistivity data plotted on logarithmic scale, emphasizing the contrast between extremely large positive MR for magnetic field perpendicular to current ($\theta = 90^\circ$) and negative MR for field parallel to current ($\theta = 0^\circ$). The upper right inset depicts the corresponding measurement configurations. The lower inset present the single crystal XRD data. (b), Magnetic field dependence of MR under various temperatures for magnetic field (μ_0H) parallel ($\theta = 0^\circ$) to the electric current (I). The inset display the original resistivity data.

Figure 1(a) displays the field dependence of MR measured at $T = 2$ K for several angles θ of the applied magnetic field (μ_0H) with respect to the electric current (I). The angle rotates from $\mu_0H//I$ to $\mu_0H \perp I$, so that at $\theta = 0^\circ$, the applied field is parallel to the current ($\mu_0H//I$), which is the so-called Lorentz force free configuration. When the magnetic field is applied perpendicular to the current ($\mu_0H \perp I$, $\theta = 90^\circ$), a positive MR of up to 10000% is observed. This large transverse MR strongly relies on θ . When the magnetic field is rotated to be parallel to the electric current ($\theta = 0^\circ$), we get a negative MR, which is an indication of chiral magnetic field and should be a strong evidence of Weyl fermions in NbAs. The left inset of Fig. 1(a) displays the original resistivity data plotted on logarithmic scale,

emphasizing the contrast between extremely large positive MR for magnetic field perpendicular to current ($\theta = 90^\circ$) and negative MR for field parallel to current ($\theta = 0^\circ$). The right inset of Fig. 1(a) depicts the corresponding measurement configurations. Fig. 1(b) presents the MR at various temperatures, when magnetic field parallel to the current ($\mu_0H//I$, $\theta = 0^\circ$). And the inset of Fig. 1(b) display the original resistivity data. Below 20 K, an negative MR of about -20% can be observed under an applied field of 3.2 T. Then, the negative MR is suppressed with increasing temperature, and ultimately disappeared at higher temperature, similar with the result in $ZrTe_5$ ²⁸ and $TaAs$ ¹⁰.

The existence of chiral quasi-particles in Dirac and Weyl semimetals opens the possibility to observe the effects of the chiral anomaly¹. The chiral magnetic effect, which is the generation of electric current in an external magnetic field induced by the chirality imbalance, is of particular interest^{9,29}. The most prominent signature of the chiral magnetic effect in Dirac systems in parallel electric and magnetic fields is the positive contribution to the conductivity that has a quadratic dependence on magnetic field^{9,30,31}. The chiral anomaly contributed conductivity as $\sigma = (e^3 v_F^3 / 4\pi^2 \hbar \mu^2 c) B^2$ where τ is the inter valley scattering time, v_F is the Fermi velocity near the Weyl points and μ denotes the chemical potential measured from the energy of the Weyl points¹⁰. This is because the chiral magnetic effect current is proportional to the product of chirality imbalance and the magnetic field, and the chirality imbalance in Dirac systems is generated dynamically through the anomaly with a rate that is proportional to the product of electric and magnetic fields $\mathbf{E} \cdot \mathbf{B}$ ²⁸. As a result, the longitudinal MR becomes negative^{30,31}, which has the maximum effect with \mathbf{E} parallel to \mathbf{B} ¹⁰. Of course the total conductivity of the system will also include other contributions from the nonchiral states as well, which may weaken the negative MR effect or even overwhelm it if the non-chiral part dominates the DC transport, which may be the case in ref.²⁴. Therefore in order to see the chiral negative MR, the high quality sample with chemical potential close enough to the Weyl point is crucial¹⁰.

At low field, the data show sharp dips. The origin of this feature is not completely understood, but which may be attributed to the WAL effect stemming from the strong spin-orbit interactions³², which dominates the transport behavior of the non-chiral states^{10,28}. When magnetic field higher than 3.2 T, the MR tend to be positive again. This behavior is very similar to the situation in Bi_xSb_{1-x} and $TaAs$ ¹⁰. One possible explanation was given by X. Huang *et al.* in Ref.¹⁰ The phenomena may due to the Coulomb interaction among the electrons occupying the chiral states. Since the degeneracy of the chiral states as well as the density of states at the Fermi level goes linearly with the magnetic field, eventually the system will approach a spin-density-wave (SDW) like instability under Coulomb interaction³³. Then at finite temperature, the strong SDW fluctuation provides an-

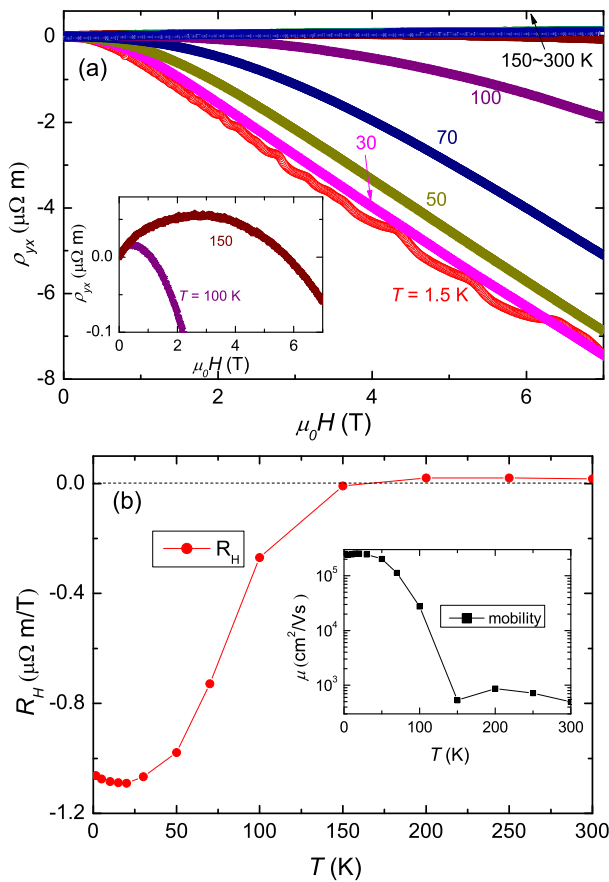


FIG. 2: (Color online) (a), Hall resistivity measured at various temperatures from 2 to 300 K. The inset displays enlarged plot of Hall resistivity curves at $T = 100$ K and 150 K. (b), Hall coefficient R_H at 7 T as a function of temperature. The inset displays mobility versus temperature determined by the Hall coefficient at 7 T and the zero field resistivity using a single band approximation.

other scattering channel which can be greatly enhanced in high field and may give the positive MR in the high field region¹⁰.

Figure 2(a) displays the magnetic field dependence of Hall resistivity $\rho_{yx}(B//c)$ measured at various temperatures. At low temperature, the negative slope in high magnetic fields indicates that the electrons dominate the main transport processes. However, in low fields the curve tends to be flat. At 100 K and 150 K, for example, ρ_{yx} is initially positive under low fields but changes to negative in higher fields. The curvature and sign reversal of the Hall resistivity indicates the coexistence of hole-type minority carriers with high mobility and electron-type majority carriers with low mobility. At higher temperature slope of Hall resistivity changes to positive, implying the carriers dominating the conduction mechanism transformed to hole-type. All these are consistent with multiple hole- and electron-like carriers as was also observed in TaAs and NbP, and indicated by band structure calculations^{10,11,21,34,35} and a previous paper on NbAs²⁴.

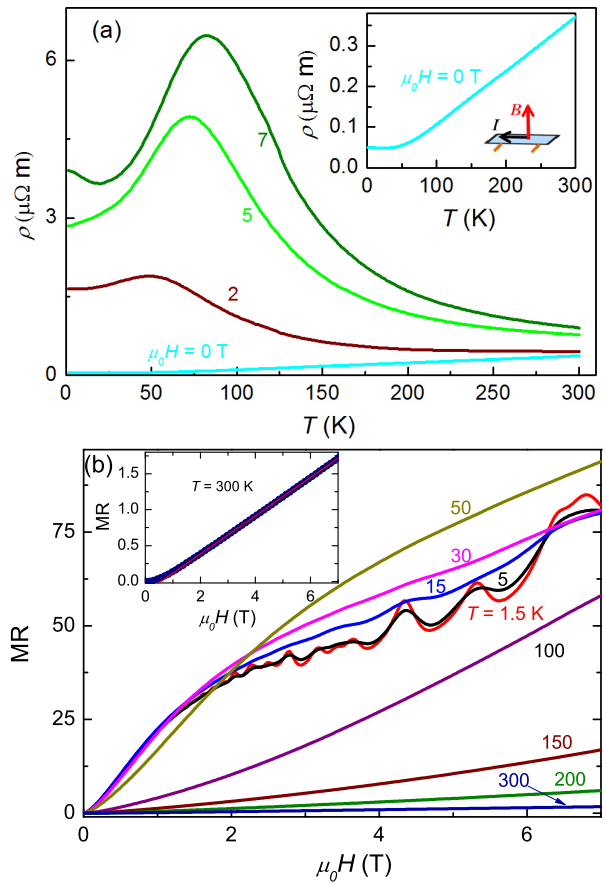


FIG. 3: (Color online) (a), The temperature dependence of resistivity in magnetic field perpendicular to the electrical current. The inset of (a) gives the measurement configuration, and zooms in on the case of 0 T. (b) Magnetic field dependence of MR at representative temperatures. The inset of (b) displays the enlarged plot for $T = 300$ K.

As shown in Fig. 2(b), the material show negative Hall coefficient, $R_H(T)$, up to 150 K and then changes sign for temperature above about 150 K. For the sake of simplicity, we use the single band to estimate the mobility. The inset of Fig 2(b) displays mobility versus temperature determined by the Hall coefficient at 7 T and the zero field resistivity using a single band approximation. The mobility plays a major role for charge transport in a material, and consequently decides the efficiency of various devices. Here, NbAs exhibits an ultrahigh mobility of $2.45 \times 10^5 \text{ cm}^2/\text{Vs}$ at 1.5 K, consistent with the result in ref.²⁴.

In Fig. 3(a) the temperature dependence of resistivity is plotted. The inset gives the measurement configuration. In zero magnetic field, NbAs exhibits a metallic behavior down to 1.5 K. The applied magnetic field not only significantly increases the resistivity, but also stimulates a crossover from metallic to insulator like behavior, which may be related to the formation of the Landau levels under magnetic field¹⁰. Under applied field, a resistivity anomaly can be observed, which can be enhanced

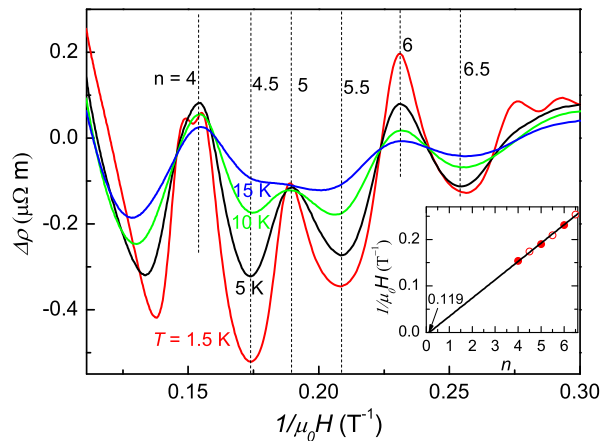


FIG. 4: (Color online) The high field oscillatory component $\Delta\rho$ plotted against inverse field $1/\mu_0 H$ at $T = 1.5, 5, 10$ and 15 K. The inset displays SdH fan diagram plotting the measured $1/B_n$ with the filling factor n , which is estimated from the $\Delta\rho$ versus $1/B_n$ plot.

and move to high temperature under higher magnetic fields. Similar behavior was observed in TaAs¹⁰, ZrTe₅ and HfTe₅¹³.

Figure 3(b) displays the field dependence of MR at various temperatures. At 300 K, the MR reaches as high as 170% at 7 T, as shown in the inset of Fig. 3(b). Above 1.5 T, the MR of our NbAs single crystal is quite linear, which is consistent with the theoretical prediction of linear quantum MR even up to the room temperature induced by 3D Dirac cone type electronic structure¹². However, the quantum limit required in Ref.¹² is actually not reached in our sample, since there is clearly more than one Landau level occupied in our field range, as will be seen in Fig. 4. Similar situations exist in multilayer epitaxial graphene³⁶, the topological insulators Bi₂Se₃ and Bi₂Te₃³⁷⁻³⁹ and Dirac Fermions Cd₃As₂²⁰. To understand the physical origin of the linear MR without reaching the quantum limit, further theoretical studies are highly desired. Nevertheless, this large room temperature linear MR is quite unusual. If its magnitude can be further enhanced, NbAs may be useful for practical applications in magnetic random access memory and magnetic sensors. At low temperatures, clear Shubnikov de Haas (SdH) oscillations have been detected starting from very weak magnetic field.

Figure 4 shows the oscillatory component of $\Delta\rho$ versus $1/B$ at various temperatures after subtracting a smooth background. They are periodic in $1/B$, as expected from the successive emptying of the Landau levels when the magnetic field is increased. The peaks marked by Landau index n are mainly stemming from the oscillations with the frequency of 25 T. The cross-sectional area of the Fermi surface (FS) $A_F = 2.38 \times 10^{-3} \text{ \AA}^{-2}$ can be obtained according to the Onsager relation $F = (\Phi_0/2\pi^2)/A_F$, where F is oscillation frequency and Φ_0 is flux quantum. We assign integer indices to the $\Delta\rho$ peak positions

in $1/B$ and half integer indices to the $\Delta\rho$ valley positions. According to the Lifshitz-Onsager quantization rule $A_F(\hbar/eB) = 2\pi(n + 1/2 + \beta + \delta)$, the Landau index n is linearly dependent on $1/B$. $2\pi\beta$ is the Berry's phase, and $2\pi\delta$ is an additional phase shift resulting from the curvature of the Fermi surface in the third direction⁴⁰. δ changes from 0 for a quasi-2D cylindrical Fermi surface to $\pm 1/8$ for a corrugated 3D Fermi surface^{20,40}. Our data points in Fig. 4 can be fitted linearly, and the linear extrapolation gives an intercept 0.119, which means a non-trivial π Berry's phase ($\beta = 1/2$) and $\delta = 0.119$ (very close to $1/8$), signaling the 3D Dirac fermion behaviors, and implying the FS associated with 25 T quantum oscillations is enclosing a Weyl point.

In the trivial parabolic dispersion case such as that involving conventional metals, the Berry's phase $2\pi\beta$ should be zero. For Dirac systems with linear dispersion, there should be a nontrivial π Berry's phase ($\beta = 1/2$). This non-trivial π Berry's phase has been clearly observed in 2D graphene^{16,17}, bulk Rashba Semiconductor BiTeI¹⁸, bulk SrMnBi₂ in which highly anisotropic Dirac fermions reside in the 2D Bi square net¹⁹, 3D Dirac Fermions Cd₃As₂²⁰, and recently in Weyl semi-metal TaAs^{10,21}. The intercept 0.119 obtained in Fig. 4 clearly reveals the nontrivial π Berry's phase, and thus provides strong evidence for the existence of Weyl fermions in NbAs. An additional phase shift $\delta = 0.119 \sim 1/8$ should result from the 3D nature of the system. Complementary to previous theoretic¹¹ and ARPES experiments result²⁵, our bulk transport measurements confirm the 3D Dirac semimetal phase in NbAs.

In summary, we have performed bulk transport measurements on single crystals of the proposed 3D Weyl semimetal NbAs. Large MR as high as 10000% is detected with magnetic field perpendicular to the current. When the external magnetic field is rotated to be parallel with the current, Chiral anomaly induced negative MR up to -20% is observed. This unusual negative MR is the first electric transport evidence for the chiral anomaly associated with the Weyl points in NbAs. Hall effect data suggest that both n and p types of carriers exist in NbAs. NbAs exhibits an ultrahigh mobility of $2.45 \times 10^5 \text{ cm}^2/\text{Vs}$ at 1.5 K. A large linear quantum magnetoresistance is observed at room temperature. By analyzing the Shubnikov de Haas oscillations of longitudinal resistance at low temperature, a nontrivial π Berry's phase with a phase shift of 0.119 is obtained, which provides bulk quantum transport evidence for the existence of a 3D Weyl semimetal phase in NbAs. With its unique electronic structure, unusual high mobility, and large room-temperature linear magnetoresistance, the 3D Weyl semimetal NbAs may open new avenues for future device applications.

This work is supported by the National Basic Research Program of China (Grant Nos. 2011CBA00103 and 2012CB821404), NSF of China (Contract Nos. 11174247 and U1332209), Specialized Research Fund for the Doctoral Program of Higher Education (Grant No.

20100101110004), and the Zhejiang Provincial Natural

Science Foundation of China (Grant. No. Y6100216).

-
- * Electronic address: phyzhengyi@zju.edu.cn
 † Electronic address: zhuan@zju.edu.cn
- ¹ H. B. Nielsen, and M. Ninomiya, *Phys. Lett. B* **130**, 389 (1983).
 - ² S. A. Parameswaran, T. Grover, D. A. Abanin, D. A. Pesin, and A. Vishwanath, *Phys. Rev. X* **4**, 031035 (2015).
 - ³ R. Lundgren, P. Laurell, and G. A. Fiete, *Phys. Rev. B* **90**, 165115 (2014)
 - ⁴ T. Ojanen, *Phys. Rev. B* **87**, 245112 (2013).
 - ⁵ A. C. Potter, I. Kimchi, and A. Vishwanath, *Nat. Commun.* **5**, 5161 (2014).
 - ⁶ P. E. Ashby, and J. P. Carbotte, *Phys. Rev. B* **87**, 245131 (2013)
 - ⁷ X. G. Wan, A. M. Turner, A. Vishwanath, and S. Y. Savrasov, *Phys. Rev. B* **83**, 205101 (2011).
 - ⁸ G. Xu, H. M. Weng, Z. Wang, X. Dai, Z. Fang, *Phys. Rev. Lett.* **107**, 186806 (2011).
 - ⁹ K. Fukushima, D. Kharzeev, and H. Warringa, *Phys. Rev. D* **78**, 074033 (2008).
 - ¹⁰ X. Huang, L. Zhao, Y. Long, P. Wang, D. Chen, Z. Yang, H. Liang, M. Xue, H. Weng, Z. Fang, X. Dai, and G. Chen, arXiv:1503.01304.
 - ¹¹ H. Weng, C. Fang, Z. Fang, B. A. Bernevig, and X. Dai, *Phys. Rev. X* **5**, 011029 (2015).
 - ¹² Z. Wang, H. Weng, Q. Wu, X. Dai, and Z. Fang, *Phys. Rev. B* **88**, 125427 (2013).
 - ¹³ T. M. Tritt, N. D. Lowhorn, R. T. Littleton, IV, A. Pope, C. R. Feger, and J. W. Kolis, *Phys. Rev. B* **60**, 7816 (1999).
 - ¹⁴ G. P. Mikitik and Y. V. Sharlai, *Phys. Rev. Lett.* **82**, 2147 (1999).
 - ¹⁵ G. P. Mikitik and Y. V. Sharlai, *Phys. Rev. Lett.* **93**, 106403 (2004).
 - ¹⁶ K. S. Novoselov, A. K. Geim, S. V. Morozov, D. Jiang, M. I. Katsnelson, I. V. Grigorieva, S. V. Dubonos, and A. A. Firsov, *Nature (London)* **438**, 197 (2005).
 - ¹⁷ Y. B. Zhang, Y. W. Tan, H. L. Stormer, and P. Kim, *Nature (London)* **438**, 201 (2005).
 - ¹⁸ H. Murakawa, M. S. Bahramy, M. Tokunaga, Y. Kohama, C. Bell, Y. Kaneko, N. Nagaosa, H. Y. Hwang, and Y. Tokura, *Science* **342**, 1490 (2013).
 - ¹⁹ J. Park, G. Lee, F. Wolff-Fabris, Y. Y. Koh, M. J. Eom, Y. K. Kim, M. A. Farhan, Y. J. Jo, C. Kim, J. H. Shim, and J. S. Kim, *Phys. Rev. Lett.* **107**, 126402 (2011).
 - ²⁰ L. P. He, X. C. Hong, J. K. Dong, J. Pan, Z. Zhang, J. Zhang, and S. Y. Li, *Phys. Rev. Lett.* **113**, 246402 (2014).
 - ²¹ C. Zhang, Z. Yuan, S. Xu, Z. Lin, B. Tong, M. Z. Hasan, J. Wang, C. Zhang, and S. Jia, arXiv:1502.00251.
 - ²² B. Q. Lv, H. M. Weng, B. B. Fu, X. P. Wang, H. Miao, J. Ma, P. Richard, X. C. Huang, L. X. Zhao, G. F. Chen, Z. Fang, X. Dai, T. Qian, and H. Ding, arXiv:1502.04684.
 - ²³ B. Q. Lv, N. Xu, H. M. Weng, J. Z. Ma, P. Richard, X. C. Huang, L. X. Zhao, G. F. Chen, C. Matt, F. Bisti, V. Stokov, J. Mesot, Z. Fang, X. Dai, T. Qian, M. Shi, and H. Ding, arXiv:1503.09188.
 - ²⁴ N. J. Ghimire, Y. Luo, M. Neupane, D. J. Williams, E. D. Bauer, and F. Ronning, *J. Phys.: Condens. Matter* **27** 152201 (2015).
 - ²⁵ S. Xu, N. Alidoust, I. Belopolski, C. Zhang, G. Bian, T. Chang, H. Zheng, V. Stokov, D. S. Sanchez, G. Chang, Z. Yuan, D. Mou, Y. Wu, L. Huang, C. Lee, S. Huang, B. Wang, A. Bansil, H. Jeng, T. Neupert, A. Kaminski, H. Lin, S. Jia, and M. Z. Hasan, arXiv:1504.01350.
 - ²⁶ S. Furuseth, and A. Kjekshuh, *Acta Crystallogr* **17**, 1077 (1964).
 - ²⁷ H. Boller, and E. Parthe, *Acta Crystallogr* **16**, 1095 (1963).
 - ²⁸ Q. Li, D. E. Kharzeev, C. Zhang, Y. Huang, I. Pletikosić, A. V. Fedorov, R. D. Zhong, J. A. Schneeloch, G. D. Gu, and T. Valla, arXiv:1412.6543.
 - ²⁹ D. E. Kharzeev, *Prog. Part. Nucl. Phys.* **75**, 133 (2014).
 - ³⁰ D. T. Son, and B. Z. Spivak, *Phys. Rev. B* **88**, 104412 (2013).
 - ³¹ A. A. Burkov, *Phys. Rev. Lett.* **113**, 247203 (2014).
 - ³² H. J. Kim, K. Kim, J. F. Wang, M. Sasaki, N. Satoh, A. Ohnishi, M. Kitaura, M. Yang, and L. Li, *Phys. Rev. Lett.* **111**, 246603 (2013).
 - ³³ J. Alicea, L. Balents, *Phys. Rev. B* **79**, 241101R (2009).
 - ³⁴ S. M. Huang, S. Y. Xu, I. Belopolski, C. C. Lee, G. Chang, B. K. Wang, N. Alidoust, G. Bian, M. Neupane, A. Bansil, H. Lin, and M. Z. Hasan, arXiv:1501.00755.
 - ³⁵ C. Shekhar, A. K. Nayak, Y. Sun, M. Schmidt, M. Nicklas, I. Leermakers, U. Zeitler, W. Schnelle, J. Grin, C. Felser, B. Yan, arXiv:1502.04361.
 - ³⁶ A. L. Friedman, J. L. Tedesco, P. M. Campbell, J. C. Culbertson, E. Aifer, F. K. Perkins, R. L. Myers-Ward, J. K. Hite, C. R. Eddy, Jr., G. G. Jernigan, and D. K. Gaskill, *Nano Lett.* **10**, 3962 (2010).
 - ³⁷ H. Tang, D. Liang, R. L. Qiu, and X. P. Gao, *ACS Nano* **5**, 7510 (2011).
 - ³⁸ See D. X. Qu, Y. S. Hor, J. Xiong, R. J. Cava, and N. P. Ong, *Science* **329**, 821 (2010).
 - ³⁹ X. Wang, Y. Du, S. Dou, and C. Zhang, *Phys. Rev. Lett.* **108**, 266806 (2012).
 - ⁴⁰ H. Murakawa, M. S. Bahramy, M. Tokunaga, Y. Kohama, C. Bell, Y. Kaneko, N. Nagaosa, H. Y. Hwang, and Y. Tokura, *Science* **342**, 1490 (2013).